




The Effects on Tsunami Hazard Assessment in Chile of Assuming Earthquake Scenarios with Spatially Uniform Slip

MATÍAS CARVAJAL¹  and ALEJANDRA GUBLER²

Abstract—We investigated the effect that along-dip slip distribution has on the near-shore tsunami amplitudes and on coastal land-level changes in the region of central Chile (29°–37°S). Here and all along the Chilean megathrust, the seismogenic zone extends beneath dry land, and thus, tsunami generation and propagation is limited to its seaward portion, where the sensitivity of the initial tsunami waveform to dislocation model inputs, such as slip distribution, is greater. We considered four distributions of earthquake slip in the dip direction, including a spatially uniform slip source and three others with typical bell-shaped slip patterns that differ in the depth range of slip concentration. We found that a uniform slip scenario predicts much lower tsunami amplitudes and generally less coastal subsidence than scenarios that assume bell-shaped distributions of slip. Although the finding that uniform slip scenarios underestimate tsunami amplitudes is not new, it has been largely ignored for tsunami hazard assessment in Chile. Our simulations results also suggest that uniform slip scenarios tend to predict later arrival times of the leading wave than bell-shaped sources. The time occurrence of the largest wave at a specific site is also dependent on how the slip is distributed in the dip direction; however, other factors, such as local bathymetric configurations and standing edge waves, are also expected to play a role. Arrival time differences are especially critical in Chile, where tsunamis arrive earlier than elsewhere. We believe that the results of this study will be useful to both public and private organizations for mapping tsunami hazard in coastal areas along the Chilean coast, and, therefore, help reduce the risk of loss and damage caused by future tsunamis.

Key words: Tsunami modeling, along-dip slip distribution, tsunami amplitude sensitivity, coastal land-level change sensitivity, tsunami hazard assessment Chile, arrival times tsunami waves.

1. Introduction

Tsunami simulation techniques have significantly improved in recent years and have become a powerful tool for tsunami hazard assessment (SATAKE 2014). Recent studies have shown that if the source parameters are well constrained, tsunami observations can be accurately reproduced by simulation tools (e.g., SATAKE *et al.* 2013; BLETERY *et al.* 2014; ARÁNGUIZ *et al.* 2016). Unfortunately, source parameters are usually either poorly constrained or unknown for earlier events, which provide the basis for tsunami hazard assessment of exposed coastal locations that have not been affected by local tsunamis in recent times.

In general, tsunami simulation is either (1) deterministic or (2) probabilistic. Unlike the former approach, the probabilistic method includes measures of uncertainty in rupture heterogeneity and the likelihood of the event occurring (GEIST and PARSONS 2006; GONZÁLEZ *et al.* 2009). However, the deterministic approach is widely used in tsunami hazard assessment because of its simplicity in implementation (e.g., OKAL *et al.* 2006; HEIDARZADEH *et al.* 2008; WITTER *et al.* 2013). This is the case for tsunami hazard maps developed for the coastal locations of Chile, a region which overlies an >3000 km long megathrust that has recently shown its tsunami potential by producing three great (Mw >8) tsunamigenic earthquakes (2010, 2014, and 2015) in 6 years.

Typically, the deterministic method involves the computation of tsunami inundation from (1) a maximum credible earthquake, with parameters based on historical and geological evidence of the past events or (2) a series of source scenarios that include

¹ Escuela Ciencias del Mar, Pontificia Universidad Católica de Valparaíso, Valparaíso, Chile. E-mail: matias.carvajal.ramirez@gmail.com

² Departamento de Obras Civiles, Universidad Técnica Federico Santa María, Valparaíso, Chile.

uncertainties in the earthquake rupture characteristics. In Chile, tsunami hazard maps have been generally developed using the former approach, where maximum credible earthquakes are based on historical events (SHOA 2015). In this case, the source parameters are usually obtained from seismic moment estimates of previous studies that are based on seismic and tsunami data, as well as on written records (e.g., LOMNITZ 1970; KELLEHER 1972; BECK *et al.* 1998; BARRIENTOS 2007). Because rupture characteristics are usually unknown, the initial tsunami wave field is computed from the seafloor vertical displacement produced by the elastic dislocation of a rectangular source plane with uniform slip, where the amount of slip is derived from the estimated seismic moment and scaling laws (SHOA 2015).

Although direct observations of co-seismic slip patterns are non-existent, slip distributions inferred for recent megathrust events suggest that slip is rarely uniformly distributed on the fault. In a real megathrust earthquake, co-seismic slip must terminate more gradually because of the velocity-strengthening behavior of the up-dip and down-dip transition zones that limit the seismogenic zone (WANG and HE 2008; HU and WANG 2008). This is supported by inversions of geodetic (e.g., MORENO *et al.* 2009), seismic (e.g., LAY *et al.* 2010), and tsunami (e.g., HEIDARZADEH *et al.* 2016) observations, which typically suggest bell-shaped distributions of slip roughly symmetrical in the dip direction (Fig. 1c). Such bell-shaped patterns are consistent with crack theory (e.g., GEIST and DMOWSKA 1999) and both analog (e.g., ROSENAU *et al.* 2010) and fault friction (e.g., WANG and HE 2008) models.

It is well known that tsunami models that prescribe uniform slip in the dip direction underestimate tsunami inundation on land (GEIST and DMOWSKA 1999). Source scenarios that involve uniform slip tend to predict smaller tsunami amplitudes and leading wave steepness than scenarios with bell-shaped distributions, and thus underestimate tsunami run up (GEIST and DMOWSKA 1999; GEIST 2002; RUIZ *et al.* 2015). As we will show, this difference is enlarged when the simulations are performed in the region of Chile, where a significant portion of the megathrust lies beneath dry land (OMIRA *et al.* 2016). Here, broader wavelengths of surface deformation, as

predicted by uniform slip models, result in excessive land deformation and less seafloor displacement, and, therefore, reduces the overall size of the tsunami at the source. Finally, land inundation is expected to be reduced even more by the underestimated coastal subsidence, or even coastal uplift, that is usually predicted by a uniform slip source.

In this paper, we present the effects on tsunami assessment in Chile of assuming earthquake scenarios with uniform slip in the dip direction. In particular, we explore the near-shore tsunami amplitudes and coastal land-level changes predicted by equal-magnitude earthquakes that involve uniform and typical bell-shaped patterns of slip. The simulations are performed on the region of central Chile (29°–37°S), where historical and geological records suggest that its central portion has not been affected by a large tsunami since 1730.

We believe that the results of this study will be useful to both public and private organizations for mapping tsunami hazard in coastal areas along the Chilean coast, and, therefore, help reduce the risk of loss and damage caused by future tsunamis.

2. Methods

2.1. Earthquake Scenarios

We investigate the effect that down-dip slip distribution has on the near-shore tsunami waves and on coastal land-level changes by means of numerical simulation methods. We performed our simulations on the actual bathymetry of central Chile, between 29° and 37°S. We chose this region for three main reasons: (1) it has a relatively large coastal population, both permanent and transient, (2) its central portion has not had a large tsunamigenic earthquake since 1730 (e.g., LOMNITZ 1970), and (3) the recent 2010 (Mw 8.8) and 2015 (Mw 8.3) earthquakes, which ruptured the southern and northern boundaries, respectively, probably augmented the stress of the central portion interface (Fig. 1b).

For our simulations, we used the rupture area and average slip amount of the 1730 earthquake inferred by CARVAJAL and GORIGOITÍA (2015), which is consistent with written records and tsunami deposits (Fig. 1b). The rupture involves 10 m of average slip

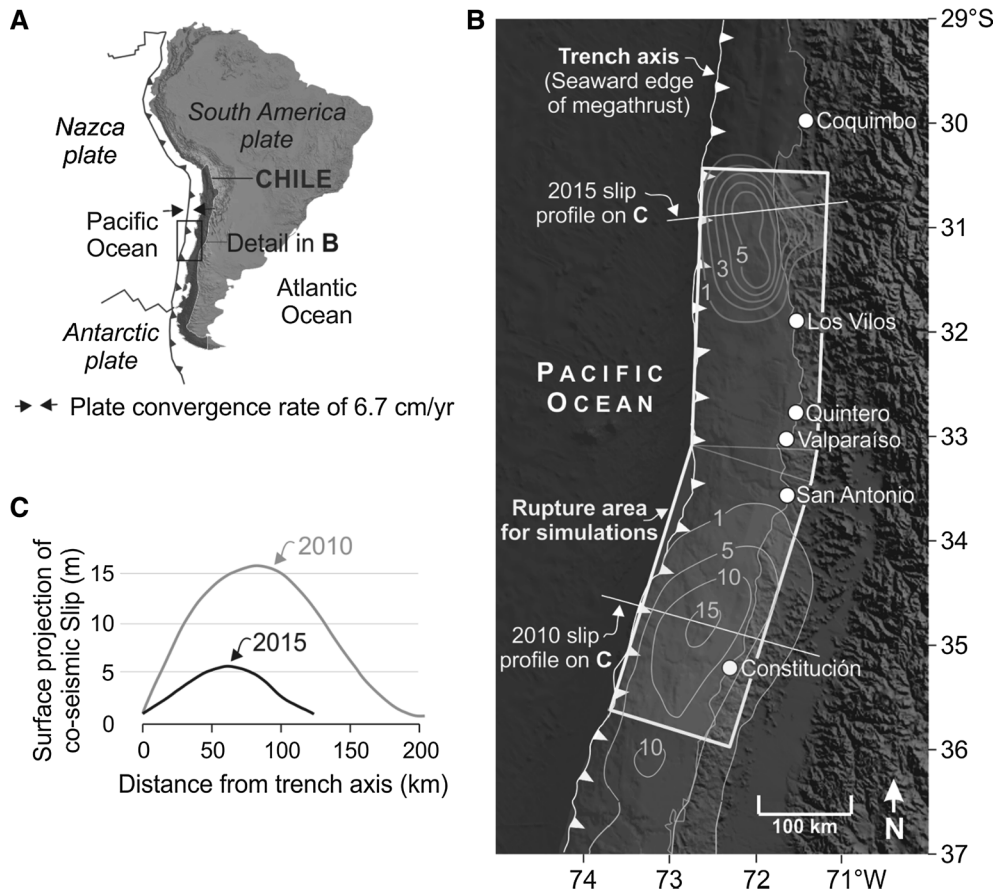


Figure 1

Index maps and recent central Chile earthquakes. **a** Tectonic setting of Chile. **b** Study area of central Chile. *Contour lines* indicate inferred slip of the 2015 (1-m slip contour intervals) and 2010 (5-m slip contour intervals) earthquakes (TILMANN *et al.* 2015; MORENO *et al.* 2012, respectively). The polygonal area indicates the inferred rupture area of the 1730 Mw ~ 9 earthquake (CARVAJAL and GORIOITIA 2015), which is used in the simulations. **a** Profiles of the surface projection of the 2015 and 2010 slip

on a 600×150 km fault area, simulating an Mw 9.0 earthquake. The along-strike length is centered at $\sim 33^\circ\text{S}$, and the along-dip width extends to the trench, as expected for large earthquakes (LAY *et al.* 2012). The rupture area is represented by two main rectangular segments of 300 km long that are parallel to the trench axis (seaward edge of megathrust), with strike angles of 3° and 25° for the northern and southern segments, respectively. We filled the triangle-shaped gap, formed between the main segments, by adding small rectangular faults. For simplicity, we represented the curved megathrust geometry by a planar fault dipping at 15° , according to the average dip angle of the central Chile megathrust (TASSARA and ECHAUREN 2012). Although this simplified fault

geometry is also expected to affect the initial tsunami wave profile, its effects are small relative to those produced by along-dip variations of slip (e.g., GODA *et al.* 2014). In the dip direction, we divided the tsunami source into 15 segments of 10 km wide to allow for non-uniform distributions of earthquake slip. We fixed the slip angle at 90° , to assume pure dip-slip faulting.

We constructed four equal-magnitude earthquake scenarios that differ in how the slip is distributed along the dip direction (Fig. 2a). The scenarios include an earthquake that involves a uniform distribution of slip and three others that have typical bell-shaped slip patterns, but differ in the depth range of slip concentration. All the scenarios are prescribed with 10 m of

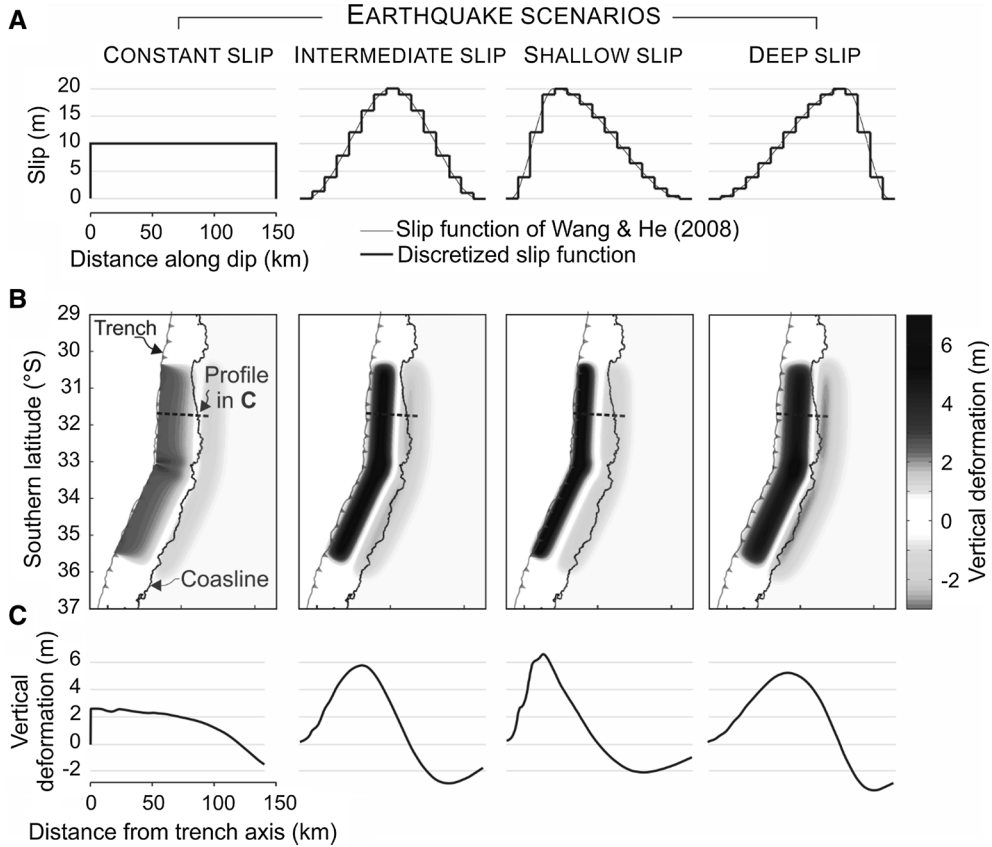


Figure 2

Earthquake scenarios considered in this study. **a** Discretized slip distributions in the dip direction used in the simulations. **b** Vertical deformation field of each scenario. **c** Cross-sectional profiles perpendicular to the fault strike of surface vertical deformation (and the initial waveform profile) of each scenario

average slip, and their slip patterns are evenly distributed in the strike direction. Our bell-shaped scenarios follow a discretized version of the slip function of WANG and HE (2008) modified from the slip distribution of FREUND and BARNETT (1976). This function allows the slip to decrease in both the up-dip and down-dip directions, as expected to occur at real megathrust earthquakes (WANG and HE 2008). After correcting some typographical errors found first by WANG *et al.* (2013), the slip function is defined as follows:

$$S(x') = S_0 \delta [1 + \sin(\pi \delta^b)] \quad (1)$$

$$\delta(x') = \begin{cases} \frac{6}{q^3} x'^2 \left(\frac{q}{2} - \frac{x'}{3}\right), & 0 \leq x' \leq q \\ \frac{6}{(1-q)^3} (1-x')^2 \left(\frac{1-q}{2} - \frac{1-x'}{3}\right), & q \leq x' \leq 1 \end{cases} \quad (2)$$

Here, $x' = x/W$, where x is the down-dip distance from the trench axis and W is down-dip width, S_0 is maximum slip, b is a broadness parameter ranging from 0 to 0.3 (here, we used 0.25), and q is a skewness parameter ranging from 0 to 1.

From function (1) and (2), we built three bell-shaped scenarios that reflect the depth-varying rupture properties of a real megathrust (LAY *et al.* 2012). We simulate a shallow, intermediate, and deep slip earthquake scenario (Fig. 2a) with varying depth range of slip concentration, by assigning skewness parameter q values of 0.25, 0.50, and 0.75, respectively (lower values of q cause the bell shape to skew up-dip).

2.2. Simulation of Tsunamis and Coastal Land-Level Changes

Both the coastal land-level changes and the initial condition for tsunami propagation for each slip scenario are provided by the co-seismic vertical surface displacement field that results from fault dislocation. Because the water is incompressible and the rupture is assumed to occur instantaneously (KAJURA 1970), the initial tsunami wave field mimics the seafloor deformation. Seafloor and land deformations were computed by the analytical solutions of a rectangular source given by OKADA (1985). To account for the along-dip variations of slip, the total surface deformation was approximated by superimposing the displacements of uniform slip dislocations of individual fault segments (GEIST and DMOWSKA 1999).

The propagation of tsunami waves was computed using a finite-difference method on actual bathymetry. We use the well-validated numerical model COMCOT, which solves the linear and non-linear shallow water equations using a leap frog scheme on a staggered and nested grid system (WANG 2009). We represented the bathymetry of central Chile by a single-level grid with 30 arc sec of spatial resolution, constructed from GEBCO bathymetry (IOC *et al.* 2003).

We computed the tsunami simulations at the 50-m water depth contour, to exclude the uncertainty associated with the hydrodynamics at shallow depths (SHUTO 1991; GEIST 2002). Computing tsunami propagation and runup in water shallower than 50 m strongly increases the uncertainty of the results, and needs additional requirements, such as detailed coastal topo-bathymetry and the addition of non-linear terms and bottom friction coefficients (SHUTO 1991).

We also investigated the effect that along-dip slip distribution has on the arrival times of both the leading and largest wave, by computing 2 h of tsunami amplitudes at two synthetic tide gauges located at the bays of Valparaíso (71.619°W, 33.036°S) and Quintero (71.512°W, 32.777°S). To better represent the bays' bathymetric features, we used nautical charts to locally construct a two-level nested grid system of higher resolution (6 and 3 arc

sec). We represented the bottom friction effect by considering a Manning's roughness coefficient of 0.013.

3. Results and Discussion

The co-seismic surface vertical deformation fields, due to the fault dislocation of each of the slip scenarios considered, are shown in Fig. 2b. It is evident that an earthquake scenario that assumes uniform slip predicts vertical deformation patterns that are remarkably different than those that assume bell-shaped patterns. This is seen more clearly in the cross-sectional profiles shown in Fig. 2c (the slight undulations near the trench are associated with discretization of fault slip). Deformation patterns predicted by uniform slip scenarios exhibit lower amplitude and a broader uplift zone than bell-shaped scenarios. While the broader spatial wavelength has a direct effect on the co-seismic coastal land-level changes, the deformation peak amplitude appears to control the tsunami height at the coast.

3.1. Effects on Coastal Land-Level Changes

Whether the coast lowers or rises during an earthquake depends on the slip scenario assumed together with its normal distance to the trench. Figure 3a shows the coastal land-level changes predicted by each of the slip sources along the study area. In general, a uniform slip source predicts less coastal subsidence (>-1.5 m) than bell-shaped scenarios (>-2.5 m), but it also predicts coastal uplift in areas where the coastline gets closer to the trench, such as in the regions immediately south of Valparaíso (<1 m) and between Los Vilos and Coquimbo (<1.5 m; shadow areas in Fig. 3a). Coastal uplift of <1.3 and <2.8 m, respectively, is also predicted in these regions by the deep slip scenario (shadow areas in Fig. 3a). The intermediate and shallow slip sources systematically predict coastal subsidence (>-2.5 m) along the entire study area. Because co-seismic coastal deformations occur before the tsunami arrives to the coast, land inundation is expected to increase for these latter slip scenarios.

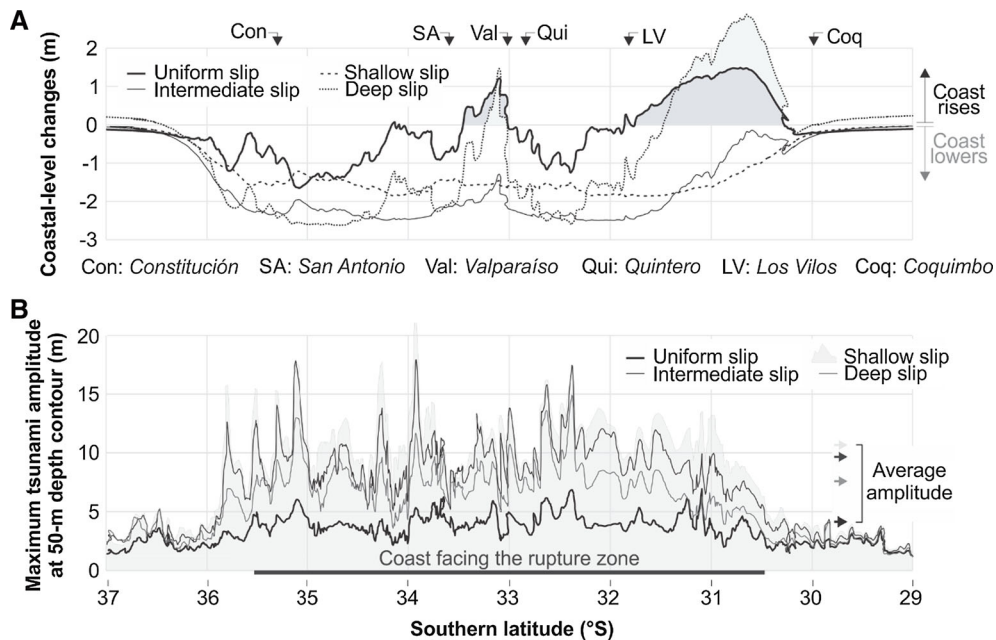


Figure 3

Alongshore profiles of coastal land-level changes and maximum tsunami amplitudes. **a** Co-seismic coastal land-level changes of central Chile's coastline predicted by each scenario, where the *shadow area* indicates coastal uplift and *arrows on top* indicate locations of sites shown in Fig. 1b. **b** Peak tsunami amplitudes along the 50-m depth contour for each scenario. *Horizontal arrows on the right* represent the average peak tsunami amplitude predicted in front of the rupture zone (*horizontal bold black line*)

3.2. Effects on Near-Shore Tsunami Amplitudes

Figure 3b shows the maximum tsunami amplitudes predicted along the 50-m depth contour by each slip scenario, revealing large differences between the tsunamis produced by the uniform slip source and those produced by bell-shaped slip scenarios. As expected by the amplitude differences on the initial tsunami waveforms among the slip scenarios (Fig. 2c), the uniform slip source predicts significantly smaller tsunami amplitudes than the bell-shaped sources. Although the average of the maximum amplitudes predicted in front of the rupture area (30.5°–35.5°S) by the bell-shaped scenarios is only about twice that produced by the uniform slip source, peak amplitudes are as much as four times larger for some sites. For example, peak amplitudes predicted south of San Antonio are ~5, ~18, ~20, and ~12 m, for the uniform, intermediate, shallow, and deep slip scenarios, respectively (Fig. 3b). Among the bell-shaped slip sources, the shallow scenario predicts the largest tsunami amplitudes at the 50-m

depth contour, while the deep scenario predicts the lowest. This is partially explained by (1) the loss of seafloor displacement in land deformation of the deep source and (2) the slip concentration of the shallow source at the up-dip portion of the seismogenic zone, where, according to Green's law, the greater ocean depth produces larger coastal tsunami amplification (GEIST 2002).

Although the finding that uniform slip scenarios underestimate tsunami amplitudes is not new (GEIST and DMOWSKA 1999; RUIZ *et al.* 2015), it has been largely ignored for tsunami hazard assessment in Chile. As mentioned in the introduction, tsunami hazard at the national level has been systematically mapped by assuming earthquake scenarios with uniform slip (SHOA 2015). Because land inundation in a specific site is determined by the tsunami amplitude that arrives at the co-seismically uplifted or subsided coast, a uniform slip scenario that underestimates both the tsunami amplitudes and the coastal subsidence consequently produces less

tsunami inundation on land. Moreover, runup is expected to be further underestimated by the less steep leading wave that is predicted by a uniform slip source (GEIST and DMOWSKA 1999).

3.3. Effects on Arrival Times of Leading and Largest Tsunami Wave

Figure 4 shows 2 h of the tsunami amplitudes predicted at Valparaíso (upper panel) and Quintero (lower panel) by each of the slip scenarios. Because the position of peak slip along dip (Fig. 2a) controls the position of peak seafloor deformation (Fig. 2c), the peak amplitudes of the leading waves occur at different times after the earthquake. Peak amplitudes of the first waves at Valparaíso occur at 19, 16, 18, and 15 min after the earthquake for the uniform, intermediate, shallow, and deep slip scenarios, respectively (upper panel of Fig. 4). Thus, in Valparaíso, the uniform slip scenario predicts later timings, of up to 4 min, of the leading wave's peak amplitude than bell-shaped slip sources. However, at Quintero, this difference decreases to 2 min. Here, peaks occur at 17 min for the uniform scenario and at

16, 18, and 15 min for the intermediate, shallow, and deep slip scenarios, respectively (lower panel of Fig. 4). Although small, these arrival time differences (2–4 min) are critical information for decision makers responsible for disaster mitigation and tsunami warning, especially in the Chilean Margin. Because, here, the trench to coast distance is significant smaller than elsewhere, tsunami waves arrive earlier to the coast, as it was evidenced in the recent 2015 tsunami when the first waves arrived to some locations in less than 15 min after the earthquake shaking (ARÁNGUIZ *et al.* 2016).

The synthetic records also reveal that the arrival time to a specific site of the largest wave is determined by the slip scenario assumed. For the case of Valparaíso, the leading wave coincides with the largest wave only for the intermediate and shallow slip sources. However, for the uniform and deep slip sources, the largest wave corresponds to the fourth wave that arrives to Valparaíso, about 1 h after the earthquake (upper panel of Fig. 4). In the Quintero case, the largest wave for all scenarios is coincident with the leading wave. The variability in the results among the bays reveals another issue in

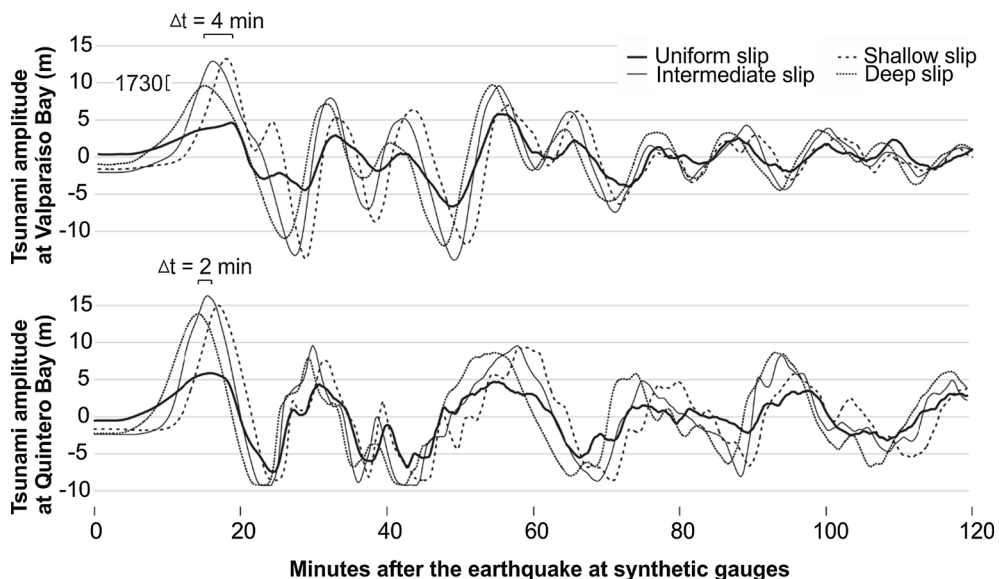


Figure 4

Synthetic marigrams at Valparaíso (*upper panel*) and Quintero (*lower panel*). Δt is the time difference of the leading wave between the uniform and deep source. Vertical bracket in the upper panel indicates the range of the 1730 tsunami runup inferred from written records (CARVAJAL and GORIGOIÍA 2015)

assuming earthquake scenarios with spatially uniform slip. The broader spatial wavelength produced by the dislocation of a uniform source (Fig. 2c) results in relatively different spectral characteristics of the initial tsunami waveform, which in turn is expected to affect the site response to the tsunami waves (RABINOVICH 2009), and thus the occurrence time of the largest wave. Other hydrodynamic sources, however, such as standing edge waves, might also play a role in the arrival time of the largest wave (YAMAZAKI *et al.* 2013). Reliable estimations of late arrival of local largest waves are important information for the timing of tsunami warning cancellations.

4. Conclusions and Recommendations

Through numerical simulation techniques, we investigated the effect that along-dip slip distribution has on the near-shore tsunami waves and on coastal land-level changes in the region of central Chile (29°–37°S). We also examined the effects on the arrival times of the leading and largest wave at two bays located within the source region (Valparaíso and Quintero). We considered four distributions of earthquake slip in the dip direction, including scenarios with spatially uniform slip and others with typical bell-shaped slip patterns. The bell-shaped sources comprise a shallow, an intermediate, and a deep scenario that differ in the depth range of slip concentration.

We found that both the coastal land-level changes and the near-shore tsunami amplitudes are remarkably sensitive to the along-dip slip distribution and that a uniform slip scenario predicts much lower tsunami amplitudes and less coastal subsidence than earthquake scenarios that account for bell-shaped patterns of slip. Among the bell-shaped slip sources, the shallow scenario predicts the largest tsunami amplitudes at the 50-m depth contour, while the deep scenario predicts the lowest.

Our simulations results also suggest that arrival times of both the leading and largest wave, depend on the slip scenario assumed. Source scenarios with uniform slip will tend to predict later arrival times (up to a few minutes) of the leading wave than bell-shaped sources. This is particularly true when comparing with

the deep scenario, which concentrates slip closer the coast. The occurrence of the largest wave at a specific site is also dependent on how the slip is distributed in the dip direction. However, local bathymetric configurations and other sources, such as standing edge waves, are also expected to play a role in the time occurrence of the largest wave.

The results of this study highlight the importance of along-dip slip when assessing tsunami hazards in Chile through deterministic methods. Bell-shaped distributions of slip, as usually inferred for recent large (and smaller) earthquakes, clearly provide more conservative estimates for tsunami hazard assessment and, therefore, should be taken into account in future studies. In the same way, previous studies based on spatially uniform slip scenarios should be reviewed and updated.

In this study, our goal was to reveal the effects of incorrectly assuming earthquake scenarios with uniform slip for tsunami hazard assessment in Chile, and not to provide precise values of tsunami amplitudes or coastal land-level changes that are expected to occur in future megathrust earthquakes. Additional requirements, such as a refined grid with high-resolution in shallow bathymetry, must be considered. Although not as crucial as the along-dip slip distribution, a better representation of the curved megathrust must also be considered to reduce the uncertainties associated with simplified planar fault geometries, such as the one used here. Similarly, tsunami planners must be aware that the scenarios with bell-shaped slip distributions used in this study do not span the full range of tsunamigenic rupture scenarios that may be geologically possible in the Chilean megathrust, such as splay fault triggering or tsunami earthquakes. Assessing tsunami hazard due to future Chilean megathrust earthquakes must consider a multidisciplinary approach based on current knowledge of tsunami source specification, generation, propagation, and inundation.

Acknowledgments

We thank the Master programs at both the Escuela Ciencias del Mar of the Pontificia Universidad Católica de Valparaíso (M. Carvajal) and the Departamento de

Obras Civiles of the Universidad Técnica Federico Santa María (A. Gubler) for their permanent support. The second author thanks CONICYT (Chile) for its FONDAF No. 15110017 (CIGIDEN). We also thank the Chilean Navy Hydrographic and Oceanographic Service (SHOA) for providing the nautical charts of Valparaíso and Quintero. We gratefully thank Dr. Frank González, an anonymous reviewer, and Cyril Mokrani for their comments, suggestions, and advices that significantly improved the manuscript.

REFERENCES

- ARÁNGUIZ, R., GONZÁLEZ, G., GONZÁLEZ, J., CATALÁN, P., CIENFUEGOS, R., YAGI, Y., OKUWAKI, R., URRÁ, L., CONTRERAS, K., DEL RIO, I., and ROJAS, C. (2016), *The 16 September 2015 Chile Tsunami from the Post-Tsunami Survey and Numerical Modeling Perspectives*. Pure Appl. Geophys., 173 (2), 333–348.
- BARRIENTOS, S. (2007), Earthquakes in Chile. In MORENO, T. and GIBBONS, W. Ed. The Geology of Chile. Geological Society of London, 2007, p. 263–287.
- BECK, S., BARRIENTOS, S., and KAUSEL, E. (1998), *Source characteristics of historic earthquakes along the central Chile subduction zone*. J. S. Am. Earth Sci., 11(2), 115–129.
- BLETERY, Q., SLADEN, A., DELOUIS, B., VALLÉE, M., NOCQUET, J.M., ROLLAND, L., and JIANG, J. (2014), *A detailed source model for the Mw9.0 Tohoku-Oki earthquake reconciling geodesy, seismology, and tsunami records*. J. Geophys. Res. Solid Earth, 119. doi:10.1002/2014JB011261.
- CARVAJAL, M., and GORIGOITÍA, N. (2015), Size of the unusual 1730 central Chile earthquake, constrained by written records and tsunami deposits. XIV Congreso geológico Chileno, La Serena, Chile, p 344–347.
- FREUND, L.B., and BARNETT, D.M. (1976), *A two-dimensional analysis of surface deformation due to dip-slip faulting*: Bull. Seismol. Soc. Am., v. 66, p. 667–675.
- GEIST, E. L., and DMOWSKA, R. (1999), *Local tsunamis and distributed slip at the source*, Pure Appl. Geophys. 154, 485–512.
- GEIST, E. (2002), *Complex earthquake rupture and local tsunamis*, J. Geophys. Res., 107(B5), ESE 2–1–ESE 2–15. doi:10.1029/2000JB000139.
- GEIST, E. L., and PARSONS, T. (2006), Probabilistic Analysis of Tsunami Hazards, Nat. Hazards, 37 (3), 277–314.
- GODA, K., MAI, P.M., YASUDA, T., and MORI, N. (2014), *Sensitivity of tsunami wave profiles and inundation simulations to earthquake slip and fault geometry for the 2011 Tohoku earthquake*. Earth Planets Space, 66(1), 1–20.
- GONZÁLEZ, F.I., GEIST, E.L., JAFFE, B., KÁNOĞLU, U., MOFIELD, H., SYNOLAKIS, C.E., TITOV, V.V., ARCAS, D., BELLOMO, D., CARLTON, D., HORNING, T., JOHNSON, J., NEWMAN, J., PARSONS, T., PETERS, R., PETERSON, C., PRIEST, G., VENTURATO, A., WEBER, J., WONG, F., and YALCINER A. (2009), *Probabilistic tsunami hazard assessment at Seaside, Oregon for near-and far-field sources*. J. Geophys. Res., 114, C11023.
- HEIDARZADEH, M., PIROOZ, M.D., ZAKER, N.H., and SYNOLAKIS, C.E. (2008), *Evaluating tsunami hazard in the northwestern Indian Ocean*. Pure Appl. Geophys., 165(11–12):2045–2058.
- HEIDARZADEH, M., MUROTANI, S., SATAKE, K., ISHIBE, T., and GUSMAN, A.R. (2016), *Source model of the 16 September 2015 Illapel, Chile, Mw 8.4 earthquake based on teleseismic and tsunami data*, Geophys. Res. Lett., 43. doi:10.1002/2015GL067297.
- HU, Y., and WANG, K. (2008), *Coseismic strengthening of the shallow portion of the subduction fault and its effects on wedge taper*, J. Geophys. Res., 113, B12411. doi:10.1029/2008JB005724.
- IOC, IHO, BODC. (2003), The Centenary Edition of the GEBCO digital atlas (CD-ROM).
- KAJIURA, K. (1970), *Tsunami source, energy and the directivity of wave radiation*. Bull. Earthq. Res. I. Tokyo. University of Tokyo, 48, 835–869.
- KELLEHER, J.A. (1972), *Rupture zones of large South American earthquakes and some predictions*. J. geophys. Res., 77(11), 2087–2103.
- LAY, T., AMMON, C. J., KANAMORI, H., KOPER, K.D., SUFRI, O., and HUTKO, A.R. (2010), *Teleseismic inversion for rupture process of the 27 February 2010 Chile (Mw 8.8) earthquake*, Geophys. Res. Lett., 37, L13301. doi:10.1029/2010GL043379.
- LAY, T., KANAMORI, H., AMMON, C.J., KOPER, K.D., HUTKO, A.R., YE, L., YUE, H., and RUSHING, T.M. (2012), *Depth-varying rupture properties of subduction zone megathrust faults*, J. Geophys. Res., 117, B04311. doi:10.1029/2011JB009133.
- LOMNITZ, C. (1970), *Major earthquakes and tsunamis in Chile during the period 1535 to 1955*, Geologische Rundschau, 59, 938–960. doi:10.1007/BF02042278.
- MORENO, M.S., BOLTE, J., KLOTZ, J., and MELNICK, D. (2009), *Impact of megathrust geometry on inversion of coseismic slip from geodetic data: Application to the 1960 Chile earthquake*, Geophys. Res. Lett., 36, L16310. doi:10.1029/2009GL039276.
- MORENO, M., MELNICK, D., ROSENAU, M., BÁEZ, J.C., KLOTZ, J., ONCKEN, O., TASSARA, A., BATAILLE, K., CHEN, J., SOCQUET, A., BEVIS, M., BOLTE, J., VIGNY, C., BROOKS, B., RYDER, I., GRUND, V., SMALLEY, R., CARRIZO, D., BARTSCH, M., and HASE, H. 2012. *Toward understanding tectonic control on the Mw 8.8 2010 Maule Chile earthquake*. E. Earth Planet. Sci. Lett., 321: 152–165.
- OKADA, Y. (1985), *Surface deformation due to shear and tensile faults in a half space*, Bull. Seismol. Soc. Am., Vol. 75, No. 4, pp. 1135–1154.
- OKAL, E. A., BORRERO, J. C., and SYNOLAKIS, C. E. (2006), *Evaluation of tsunami risk from regional earthquakes at Pisco, Peru*, B. Seismol. Soc. Am., 96(5), 1634–1648.
- OMIRA, R., BAPTISTA, M.A., and LISBOA, F. (2016), *Tsunami Characteristics Along the Peru-Chile trench: Analysis of the 2015 Mw8.3 Illapel, the 2014 Mw8.2 Iquique and the 2010 Mw8.8 Maule Tsunamis in the Near-field*, Pure Appl. Geophys., 173, pp. 1063–1077.
- RABINOVICH, A. B. (2009), Seiches and harbor oscillations. Handbook of coastal and ocean engineering, 193–236.
- ROSENAU, M., NERLICH, R., BRUNE, S., and ONCKEN, O. (2010), *Experimental insights into the scaling and variability of local tsunamis triggered by giant subduction megathrust earthquakes*, J. Geophys. Res., 115.B9, 2156–2202. doi:10.1029/2009JB007100.
- RUÍZ, J., FUENTES, M., RIQUELME, S., CAMPOS, J., and CISTERNAS, A. (2015), *Numerical simulation of tsunami runup in northern Chile based on non-uniform $k - 2$ slip distribution*, Nat. Hazards, 1–22. doi:10.1007/s11069-015-1901-9.

- SATAKE, K., FUJII, Y., HARADA, T., and NAMEGAYA, Y. (2013), *Time and Space Distribution of Coseismic Slip of the 2011 Tohoku Earthquake as Inferred from Tsunami Waveform Data*, Bull. Seismol. Soc. Am., 103(2B) 1473–1492. doi:[10.1785/0120120122](https://doi.org/10.1785/0120120122).
- SATAKE, K. (2014), *Advances in earthquake and tsunami sciences and disaster risk reduction since the 2004 Indian ocean tsunami*, Geo. Lett., 1–15. doi:[10.1186/s40562-014-0015-7](https://doi.org/10.1186/s40562-014-0015-7).
- SHOA (2015), Pub. SHOA N° 3204, Instrucciones Oceanográficas N°4, “Especificaciones Técnicas para la Elaboración de Cartas de Inundación por Tsunami (CITSU)” 1ª Edición, 2015.
- SHUTO, N. (1991), *Numerical Simulation of Tsunamis. Its past, present and near future*. Nat. Hazards, 4, pp. 171–191.
- TASSARA, A., and ECHAURREN, A. (2012), *Anatomy of the Andean subduction zone: three-dimensional density model upgraded and compared against global-scale models*, Geophys. J. Int., 189:161–168.
- TILMANN, F., ZHANG, Y., MORENO, M., SAUL, J., ECKELMANN, F., PALO, M., DENG, Z., BABEYKO, A., CHEN, K., BAEZ, J.C., SCHURR, B., WANG, R., and DAHM, T. (2015), *The 2015 Illapel earthquake, central Chile, a type case for a characteristic earthquake?*, Geophys. Res. Lett. doi:[10.1002/2015GL066963](https://doi.org/10.1002/2015GL066963).
- YAMAZAKI, Y., CHEUNG, K. F., and LAY, T. (2013), *Modeling of the 2011 Tohoku Near-Field Tsunami from Finite Fault Inversion of Seismic Waves*. Bull. Seismol. Soc. Am., 103(2B), 1444–1455.
- WANG, X. (2009), User manual for COMCOT version 1.7, first draft. Cornell University, 59 pp.
- WANG, K., and HE, J. (2008), *Effects of frictional behavior and geometry of subduction fault on coseismic seafloor deformation*, Bull. Seismol. Soc. Am., v. 98, no. 2, p. 571–579. doi:[10.1785/0120070097](https://doi.org/10.1785/0120070097).
- WANG, P. L., ENGELHART, S. E., WANG, K., HAWKES, A. D., HORTON, B. P., NELSON, A. R., and WITTER, R. C. (2013), *Heterogeneous rupture in the great Cascadia earthquake of 1700 inferred from coastal subsidence estimates*. J. Geophys. Res., 118(5), 2460–2473.
- WITTER, R. C., ZHANG, Y. J., WANG, K., PRIEST, G. R., GOLDFINGER, C., STIMELY, L., ENGLISH, J. T., and FERRO, P. A. (2013), *Simulated tsunami inundation for a range of Cascadia megathrust earthquake scenarios at Bandon, Oregon, USA*. Geosphere., 9(6), 1783–1803. doi:[10.1130/GES00899.1](https://doi.org/10.1130/GES00899.1).

(Received April 19, 2016, accepted June 10, 2016, Published online June 21, 2016)